ORIGINAL PAPER

Hydrochar-derived adsorbent for the removal of diclofenac from aqueous solution

Velma Beri Kimbi Yaah[1] · Mohamed Zbair[2] · Sérgio Botelho de Oliveira[3] · Satu Ojala[1]

© The Author(s) 2021

Abstract

The characteristics and diclofenac adsorption properties of a carbon adsorbent prepared from palm kernel shells were studied. The adsorbent prepared via hydrothermal carbonization followed by an activation in nitrogen flow had a mesoporous structure with homogenous pore distribution and the specific surface area of 131 m^2g^{-1}. The Raman spectra showed a formation of graphene or graphite structures in the material during activation with small number of defects based on its I_D/I_G ratio of about 0.5. The FTIR analysis showed both a qualitative and quantitative decrease in the functional groups of the raw material after activation. The developed adsorbent was found to be effective in the removal of diclofenac with 95% maximum removal at pH 2, adsorbent dose of 15 gL^{-1} and adsorbate dose of 50 mgL^{-1}. Diclofenac adsorption followed the Langmuir isotherm model with correlation coefficient $R^2 > 0.98$. The adsorption kinetics was explained by the second-order kinetic model with rate constant (K_2) 0.869 min^{-1}. The interaction via aromatic π–π stacking and hydrogen bonding between -OH groups of phenol and carboxylic acid groups of DCF are leading to a good adsorption efficiency despite of the low surface area of the adsorbent.

Graphic abstract
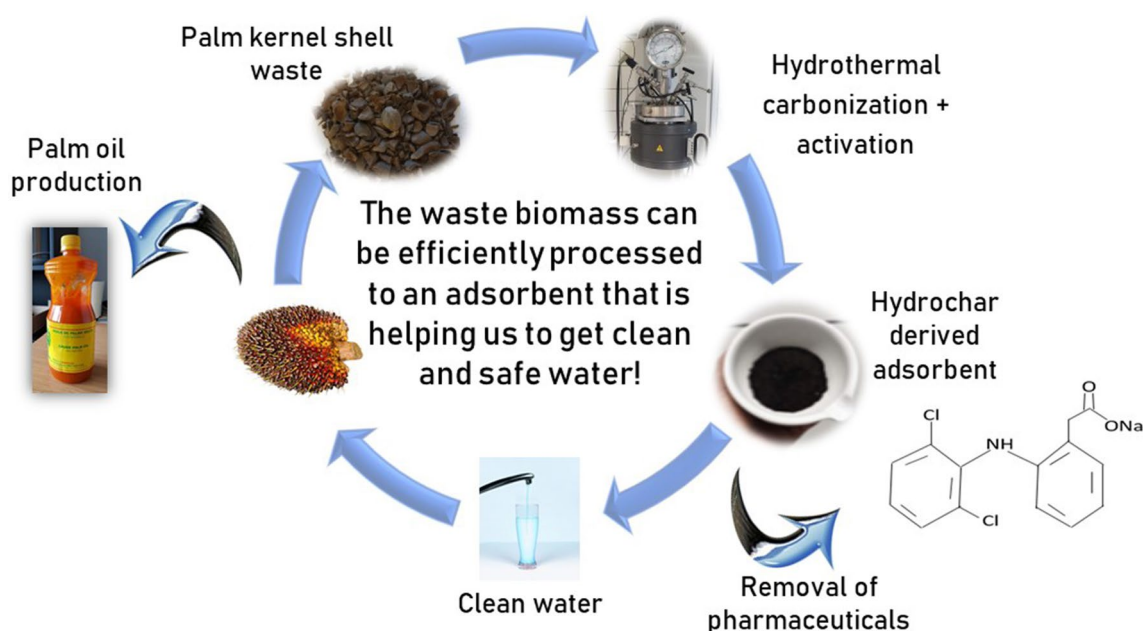
Extended author information available on the last page of the article

Springer

Introduction

Hydrothermal carbonization (HTC) is a thermochemical conversion method carried out in conditions of subcritical water, where the material is heated in a closed environment under autogenous pressure [1]. HTC has been reported to be more energy efficient and economical compared to the other thermochemical conversion processes, such as pyrolysis. HTC has no specific requirements for pressure, and the pressure is dependent on the temperature used in the process. Water is used as a solvent, and thus wet feedstock can be utilized, which saves energy that is normally used to dry the feedstock before processing [2–5]. The solid product from HTC is called as hydrochar and its properties depend on the biomass source and the reaction conditions used [6, 7]. Generally, hydrochar is non-toxic and hydrophobic. The surface chemistry, porosity, particle size and specific surface area of hydrochar are dependent on the temperature and reaction time used in HTC. Corn stove hydrochars produced at 250 °C for 4 h, and pinewood at 300 °C for 20 min, had specific surfaces areas of $4 \ m^2g^{-1}$ and $21 \ m^2g^{-1}$, respectively. The specific surface area of the hydrochar can be increased using activation. In principal, there are two types of activation—physical and chemical. Physical activation is usually carried out at higher temperatures, even greater than 900 °C, in a flow of steam, CO_2 or both, while in chemical activation, activating agents like KOH are used at room or elevated temperatures (600 °C–800 °C). Chemical activation typically leads to high specific surface areas. For example, cellulose, rye straw and glucose hydrochar-derived adsorbents produced at 240 °C reached specific surface areas of 2250, 2200 and $2219 \ m^2g^{-1}$, respectively, when using KOH as an activation chemical. Though chemical activation is faster and occurs at lower temperatures, it causes secondary pollution, and hence physical activation is more recommended [8–13]. The hydrochar surface contains typically number of oxygen-containing functional groups that have good adsorption affinity for both polar and non-polar functional groups leading to high adsorption capacity. This property might be lost from the hydrochar during the gas-phase activation intended to increase the specific surface area. Therefore, careful selection of the processing conditions is necessary.

Oil palm *(Elaeis guineensis)* is a major source of vegetable oil that is extracted from its flesh and shell. Oil palms are cultivated in South East Asia (Malaysia, Indonesia, and Thailand), Africa and several southern provinces of China. Malaysia produces about two million tons dry weight of oil palm shells annually, which are normally used as biofuels and building materials [14]. Previous research has been carried out on the use of palm shell activated carbon for adsorption of pollutants, such as heavy metals (lead, copper and nickel ions), phenol and dyes (methylene blue), in aqueous solutions [15–18]. However, less information is available related to the use of adsorbents derived from palm kernel shells in adsorption of emerging pollutants and using HTC as the primary preparation method.

There has been an increase in the level of micro-pollutants especially pharmaceuticals in the effluents of wastewater treatment plants, in sewage water, groundwater and drinking water supplies. Only about 30% of pharmaceuticals are absorbed in the human body with the rest being sent out in urine and faeces. Diclofenac is a non-steroidal anti-inflammatory drug used worldwide as analgesic, anti-arthritic compounds and for the remediation of menstrual pain of females [19–23]. It has a low solubility in water and due to its negative charge, it can easily escape from the nanofiltration unit of the water treatment plant. It is already known that its presence in the aquatic ecosystem can cause damage to fish tissue and change its biochemical functions [24, 25]. Therefore, finding an efficient technology for the removal of diclofenac from water is very important.

The objective of this work was to develop a new, efficient and economic adsorbent for the removal of diclofenac in water by using hydrothermal carbonization as the primary processing technology. Palm kernel shells were selected as the raw materials. To explain the performance of the developed adsorbent, its chemical and structural properties were characterized. The adsorption isotherms and kinetics of adsorption were evaluated to get more information on the adsorption process.

Materials and Methods

Materials

Palm kernel shells were collected from the North and South-West regions of Cameroon. The shells were washed to remove the fibres and sun dried at temperature of about 32 °C. After drying, the shells were ground and sieved to a particle size of < 84 mm.

Chemical reagents

All the chemicals used in this research were of analytical reagent grade. Diclofenac sodium salt with a molecular weight of 318.13 g mol^{-1} purchased from Sigma Aldrich, 99.5% sodium chloride and 37% hydrochloric acid from Alphatec, sodium hydroxide from Neon Commercial Ltda and 95% ethanol from Química Contemporânea Ltda were used as reagents. Diclofenac sodium salt (Fig. 1a) is typically used in pharmaceuticals since diclofenac is fat-soluble and does not easily dissolve in water. Deionized water was
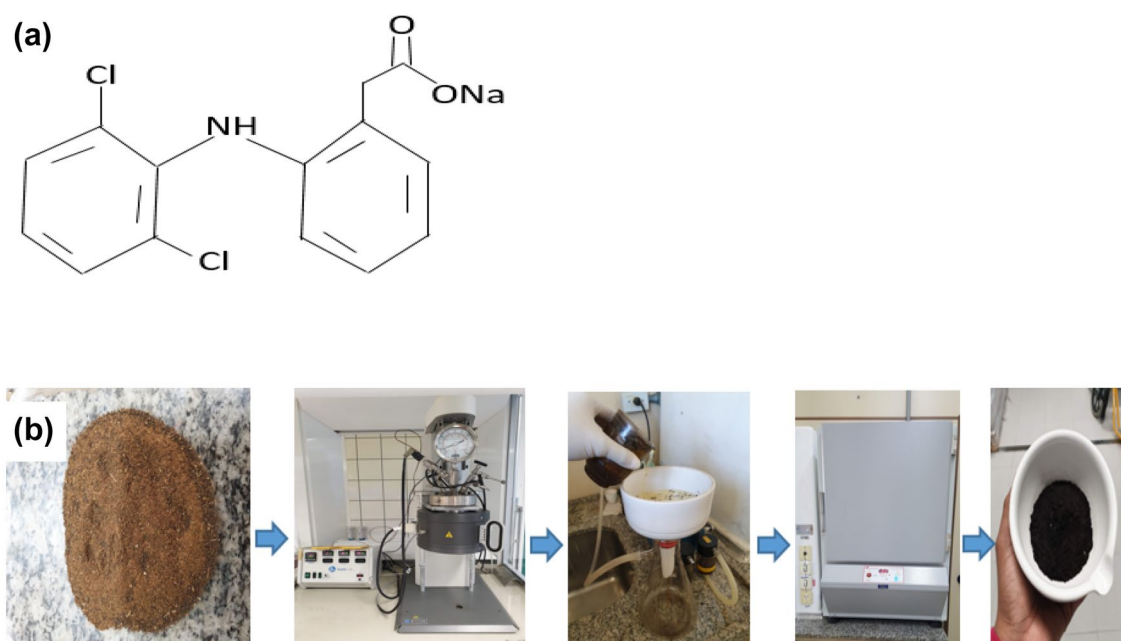
Fig. 1 **a** Chemical structure of diclofenac sodium, **b** Schematics for hydrothermal carbonization of palm kernel shells

used for the preparation of all model water solutions and as the solvent for hydrothermal carbonization.

Hydrothermal carbonization of Palm kernel shells

Hydrothermal carbonization (Fig. 1b) of palm kernel shells was done in a high-pressure Parr reactor. The reaction conditions were optimized in our earlier work and are reported in [26]. The ratio of palm kernel shells to deionized water used was 1:5. The mixture of palm kernel shells and deionized water was put in a Teflon cup with a 30% air space. The reactor was heated to 200 °C for 4 h with a heating rate of 40 °C min^{-1}. The reactor was then left to cool down, and the solid phase (hydrochar) was filtered out and dried at 80 °C for 12 h. Activation of the hydrochar was done in a nitrogen flow of 60 mL min^{-1} at 400 °C for 4 h.

Characterization

To determine the specific surface area and pore structure of the materials, nitrogen physisorption analysis (Micromeritics ASAP 2020) at −195 °C was carried out using the BET-BJH and Horvath-Kawazoe methods. The material was evacuated for 30 min at 200 °C before analysis. The morphology and structure of the palm kernel shell, hydrochar and hydrochar-derived adsorbent were analysed using a scanning electron microscopy (SEM; Jeol JSM-IT300) operated in vacuum, with electron acceleration voltage of 15 kV in backscattered electron mode. The elemental analyses were performed using the energy-dispersion spectroscopy

(EDS) technique, with Oxford Instruments X-Max N X-ray detector attached to the microscope. The Fourier transform infrared spectrometer (FTIR) (Perkin Elmer Spectrum 400) with attenuated total reflectance (ATR) accessory was used to study the functional groups on the adsorbents before and after adsorption experiments. The change in mass with temperature was analysed using thermogravimetric analysis TGA-DTG (Shimadzu DTG-60H) to evaluate the thermal stability of the hydrochar. For the analysis, the sample was placed in a 70 μL platinum crucible and heated from 25 °C to 700 °C with a heating rate of 10 °C min^{-1} under nitrogen flow of 100 mL min^{-1}. Raman spectra of the materials were obtained using the time-gated Pico Raman spectrometer (532 nm pulsed laser with a shot length of 150 ps and frequency of 40–100 kHz) from Timegate Instruments Ltd. Measurements were done in a wave number range of 100 cm^{-1} – 2100 cm^{-1}, and the wet samples were rotated during the measurements. XRD analysis of the hydrochar-derived adsorbent was realized using Rikagu SmartLab XRD device using 9 kW rotating Cu anode X-ray generator. The scanning was done at 2θ range 5–130° using a step size of 0.02°.

Adsorption experiments

Batch adsorption studies were done at several concentrations of diclofenac sodium, dosages of adsorbent, temperatures, and contact times. Each experiment was carried out in a 250 mL Erlenmeyer flask containing 100 mL volume of diclofenac solution at pH 2. The mixtures were shaken on a

SI-300R thermostat incubator shaker (Nova Analitica Imp. Exp. Ltda) at 200 rpm. Liquid samples were collected at 10, 15 and 30 min intervals, and the concentration of Diclofenac (DCF) was analysed using a UV Vis spectrometer (UV-M51) at the maximum absorbance wavelength of 276 nm. The removal percentage of diclofenac at a given time t was calculated using the Eq. 1. Equations 2 and 3 were used to calculate the amount of diclofenac adsorbed per mass unit (mg g^{-1}) of adsorbent at any given time and at equilibrium.

$$\text{Removal (\%)} = \frac{(Co - Ct)100}{Co} \tag{1}$$

$$Qt = \frac{(Co - Ct)V}{m} \tag{2}$$

$$Qe = \frac{(Co - Ce)V}{m} \tag{3}$$

In the equations, Co is initial concentration of diclofenac sodium (DCF), Ct is DCF concentration at given time, m is mass of adsorbent, Ce is equilibrium DCF concentration and V is volume of solution (L).

Langmuir (Eq. 4) [27] and Freundlich (Eq. 5) [28] models were used in examining the equilibrium data and to find out information on distribution of DCF molecules at the solid–liquid interface.

$$1/Q_e = 1/Q_{\max} + 1/(K_L Q_m C_e) \tag{4}$$

$$\text{Ln}(Q_e) = \ln K_F + 1/n \, \text{Ln}(C_e) \tag{5}$$

In the equations, C_e is concentration at equilibrium, Q_e is adsorption at equilibrium, $Q_{\max}$ is maximum adsorption capacity and K_L is Langmuir constant related to the affinity of adsorption sites for diclofenac (Lmg^{-1}), K_F is Freundlich constant, which is roughly an indicator for the sorption capacity (mgg^{-1})/(mgL^{-1}) 1/n and n is (dimensionless)

Freundlich constant indicative of the sorption intensity and heterogeneity.

Pseudo-first-order (PFO; Equation) [29] and pseudo-second-order (PSO; Eq. 7) [30] models were used in order to investigate the kinetics of the interaction between DCF and hydrochar-derived adsorbent (PKC) at the solid–liquid interface. The equations are described as:

$$\text{Ln}(Q_e - Q_t) = \log(Q_e) - K_1 t/2.303 \tag{6}$$

and

$$t/Q_t = 1/(K_2 Q_t^2) + 1/Q_e \tag{7}$$

where Q_t is adsorbed amount of diclofenac at time t, Qe is adsorption at equilibrium, K_1 and K_2 are rate constants.

Regeneration experiments

To study the reusability of the hydrochar-derived adsorbent, regeneration experiments were carried out in the following way: 1.5 g of the used material was put in 20 mL of 95% ethanol solution and shaken at 200 rpm for 4 h. After this, the adsorbent was filtered out, washed with distilled water and dried at 80 °C for 12 h. The same adsorbent was used in diclofenac adsorption and regenerated for five times.

Results and discussion

Characterization

Figure 2 shows the SEM micrographs of the dried palm kernel shells (PKS), hydrochar (PKH) and hydrochar-derived adsorbent (PKC) at 2000 × magnification. It can be observed that pores are homogenously distributed on the surface of the dried palm kernel shells. After hydrothermal carbonization, the pores are widened. During HTC process, water density and viscosity are decreased due to the
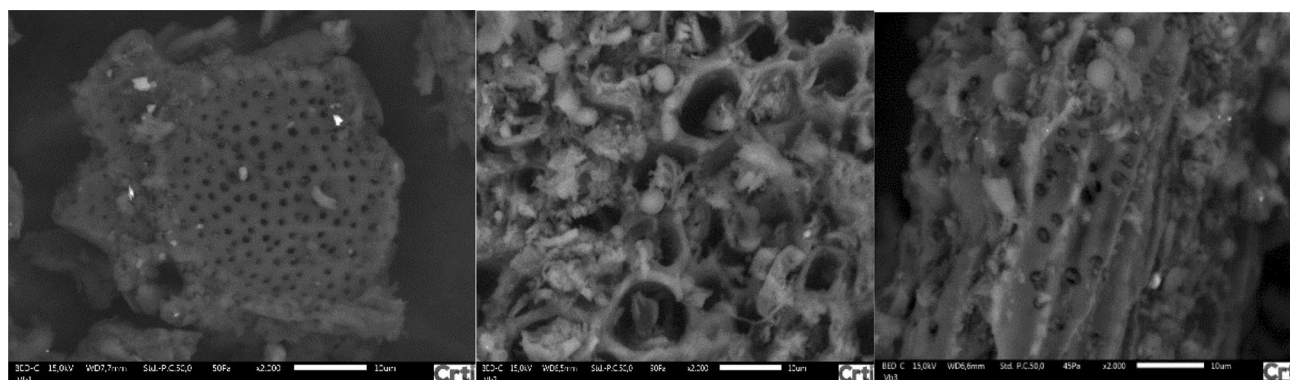

Fig. 2 SEM images for PKS, PKH and PKC at 2000 × magnification

subcritical conditions, and this is enhancing the removal of the inorganic material from the structure of the biomass while widening the pores [31]. During activation, volatile compounds are removed from the hydrochar leading to the appearance of the smaller pores [32]. This is visible in the images as well.

Based on N_2 adsorption analysis, PKC was found to be predominantly mesoporous material with specific surface area of about 131 m^2g^{-1} and the diameter of pores between 2 and 50 nm. The Horvath-Kawazoe plot showed the presence of some micropores as well. PKC had a total pore volume of 0.06 cm^3g^{-1}. The specific surface area of PKH was found to be about 22 m^2g^{-1} with presence of mesopores between diameters of 15 nm and 20 nm and macropores with diameter greater than 50 nm. The total pore volume of PKH was 0.1 cm^3g^{-1}. This result showed that a significant increase in specific surface area and modification of porous structure appears during activation.

The thermogram for the palm kernel shells shown in Fig. 3a indicates a mass loss corresponding to about 13% up to temperature of 310 °C, which is related to the loss of adsorbed water and volatile compounds. This is an endothermic process, shown by an endothermic peak observed in the DTA curve. The exothermic feature between 320 °C and 420 °C is related to a mass loss of about 24%. At this temperature range, decomposition of the functional groups with lower stability and decomposition of cellulose and hemicellulose takes place. In the temperature range between 420 °C and 700 °C, there is a mass loss of about 38% and an exothermic peak centred at around 440 °C, which is related to the decomposition of lignin [33]. This result is in accordance with the FTIR analysis where a disappearance of C=O

and C–O groups after activation of the hydrochar is observed (Fig. 3b).

The FTIR spectra of the dried palm kernel shells (PKS), palm kernel shell hydrochar (PKH), hydrochar-derived adsorbent (PKC) and the adsorbent after diclofenac adsorption (PKA) are presented in Fig. 3b. All the materials displayed bands between 3300 cm^{-1} and 3700 cm^{-1} that correspond to –OH stretching vibration [34]. The intensity of the -OH bands in untreated palm kernel shells (PKS) is lower and broader than in the case of hydrochar (PKH). The higher intensity in the latter could originate from water used in the HTC process. The C=C stretching vibrations of lignin aromatic rings around 1636 cm^{-1} and the aliphatic C–H stretching vibrations between 2923 cm^{-1} and 2852 cm^{-1} are equally observed in all the materials [35].

One can observe bands at around 1450 cm^{-1} in the spectra of PKS and PKH corresponding to the C–H deformation of lignin molecule typical for hydrochars and raw lignocellulosic materials [36]. The C=O and C–O stretching vibrations typical for saturated aliphatic compounds are present only in the PKS and PKH spectra. These groups are unstable under high temperature, which can explain the absence of these bands in the hydrochar-derived adsorbent (PKC) and PKA (after diclofenac adsorption) spectra. We also observe the C–O stretching vibration between 1240 cm^{-1} and 1230 cm^{-1} in PKS and PKH. The absence of C–O and C=O groups in PKC is also an indication of the decomposition of hemicellulose and cellulose during activation [32, 37]. In general, the activation under N_2 flow decreases the number of functional groups in the material both quantitatively and qualitatively. These functional groups play an important role in the adsorption of diclofenac on the adsorbent PKC. In the
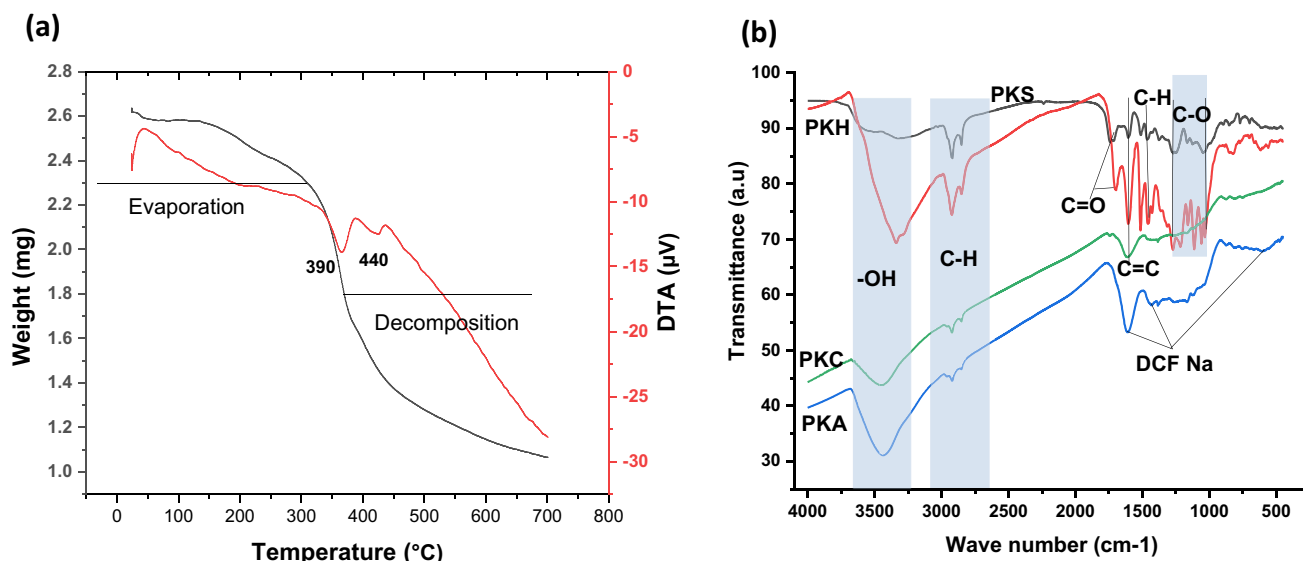

Fig. 3 **a** TGA/DTA results for the palm kernel shells, and (**b**) FTIR spectra of palm kernel shells (PKS), hydrochar (PKH), hydrochar-derived adsorbent (PKC) and after diclofenac adsorption (PKA)

PKA sample, one can observe bands at around 747 cm^{-1}, 1402 cm^{-1}, 1454 cm^{-1} and 1617 cm^{-1} all corresponding to diclofenac [38]. This proofs that diclofenac is adsorbed on the material.

The Raman spectra (Fig. 4) of the dried palm shells, hydrochar and hydrochar-derived adsorbent were used to evaluate the formation of graphite or graphene structures in the materials. Activation clearly changes the structure of the studied material. The Raman spectra show the development of D (1350 cm^{-1}) and G (1597 cm^{-1}) bands along with the activation. The D band shows the presence of defects or disorder in the graphite structure that may be beneficial for the material, while the G band is assigned to the symmetric stretching of the sp^2 graphitic carbon [39, 40]. The HTC treatment already seems to create some graphite or graphene structures to the material shown by G band. After activation, these two bands appear clearly for the PKC (I_D/I_G ratio of about 0.5), while other spectral features remain less intense. The I_D/I_G ratio of about 0.5 indicates a low amount of defects in the adsorbent. The Raman peaks below 1000 cm^{-1} are also changed during the activation. The intensities of these

peaks decrease during HTC and activation. The peaks around 1000 cm^{-1} can be attributed to the cellulose and hemicellulose components in the spectra of PKS and PKH. Decrease in intensity of these peaks is in correlation with the TGA results, which indicated the loss of the hemicellulosic and cellulosic components in the activation temperature range (~ 400 °C). Dried palm kernel shells (PKS) and hydrochar (PKH) show also spectral features in the region of C-O stretch in cellulose and hemicellulose (1056 cm^{-1}) and crystalline cellulose (1098 cm^{-1}) [41]. This ties with the FTIR results, where we observed a loss of the C–O groups after activation. We also observe prominent peaks in the Raman spectra of PKS and PKH below 900 cm^{-1} which are greatly reduced in the PKC spectrum. These peaks can be associated with hydrogen bonded to aromatic carbons [42].

Fig. 5 shows the XRD diffractogram of PKC. It is directly visible from the diffractogram, that the material is not well-structured crystalline material. Similar diffractograms are typical for biowaste-derived carbons. The broad peaks visible at 2θ 27° and at around 50° are related to the disordered graphite-like structures [43, 44], that were also observed in Raman spectra. The feature visible at around 2θ 15° could be related to graphite oxide [45, 46]. The presence of graphite oxide in material supports the information found in FTIR analysis, namely observation of various oxygen-containing functional groups.

DCF adsorption experiments

The pHpzc of the hydrochar-derived adsorbent (PKC) was determined to be 5.7 using the pH drift method [47]. The pKa of diclofenac is ~ 4.2 [19]. When the pH of the solution is equivalent to the pKa, 50% of DCF is in protonated and 50% is in deprotonated form. When pH of the solution
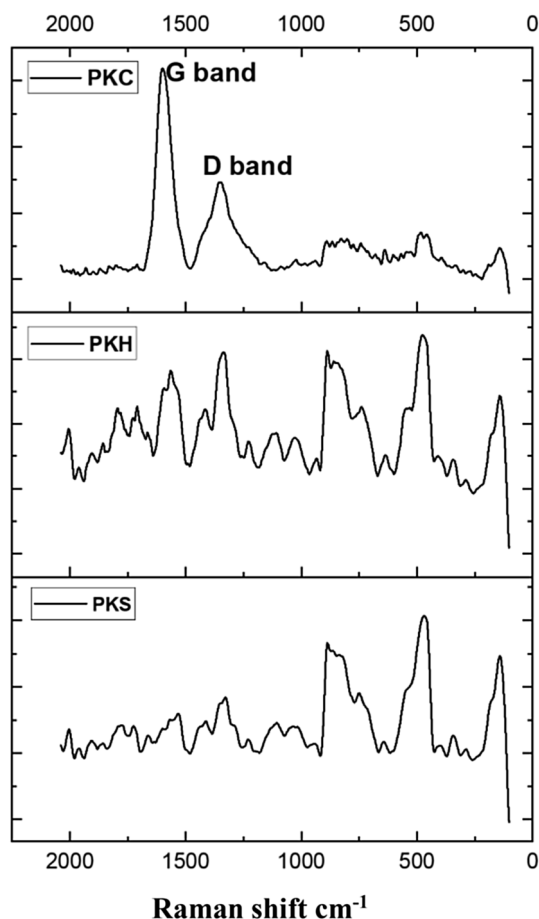

Fig. 4 Time-gated Raman spectra of dried palm kernel shells (PKS), hydrochar (PKH) and hydrochar-derived adsorbent (PKC)
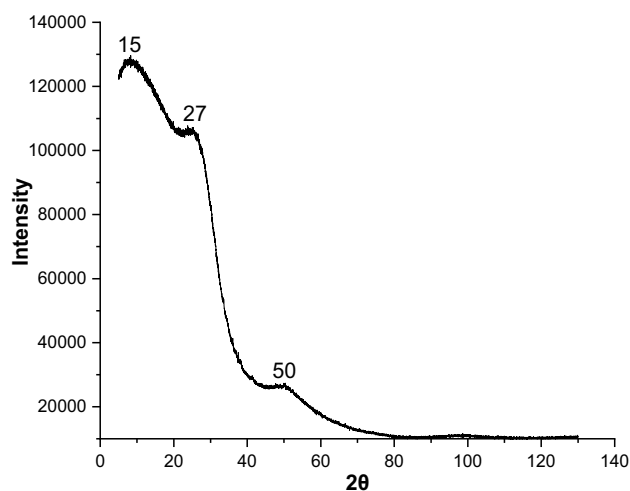

Fig. 5 XRD diffractogram of PKC

decreases, the protonated form prevails. At the pH 2, DCF is mainly in protonated form while the adsorbent surface is positively charged. After pH increases above pHpzc of the adsorbent, larger part of DCF is in deprotonated form and adsorbent has a negative charge. The lower pH (pH 2) was selected for the experiments to avoid the repulsion between the adsorbate and the adsorbent surface. Furthermore, earlier studies indicate pH 2 as optimal pH for diclofenac adsorption [19].

The effect of adsorbent amount in DCF removal was studied using 0.25, 0.5, 1.0 and 1.5 g of hydrochar-derived adsorbent (PKC). The results are presented in Fig. 6a. The adsorption of DCF on PKC after 90 min in presence of 0.25 g and 1.5 g of adsorbent was 0.214 mg g^{-1} and 0.376 mg g^{-1}, respectively. The adsorption capacity of PKC increased with increasing adsorbent mass, which is due to availability of higher number of surface sites for adsorption. Figure 5a displays that the removal of DCF increases with increasing adsorbent mass. However, when the mass of adsorbent is taken into account when calculating the amount of DCF adsorbed at a given time, the difference is not anymore equally large, which is visible in Fig. 6b. About 43% of DCF is removed during 90 min using 1.5 g of adsorbent compared to 5% removal achieved with 0.25 g of adsorbent. Usually, adsorption capacity and efficiency are linked to contact time and thus adsorption increases with increasing contact time until the adsorption–desorption process reaches the equilibrium. Based on the results, an amount of 1.5 g of adsorbent was selected for further experiments. An increase in the concentration of DCF increases the DCF removal percentage from about 75% removal at 5 ppm to maximum removal of about 95% with 50 ppm of DCF solution (Fig. 6c).

Adsorption kinetics of DCF was examined by fitting two kinetic models to the data (Fig. 7). Compared to pseudo-first-order (PFO) model, pseudo-second-order (PSO) kinetic model explained better the experimental data with the correlation coefficients (R^2) superior than 0.93 for all the studied adsorbent amounts (Table 1). The theoretical values of adsorption quantity at equilibrium ($Q_{e,cal}$ (mgg^{-1})) determined from PSO model were consistent with the experimental value ($Q_{e,exp}$ (mgg^{-1})) (see Table 1). The highest equilibrium adsorption capacity was observed for 1.5 g of adsorbent for the removal of DCF. The increase in adsorbent mass accelerated the adsorption of DCF onto adsorbent, which was shown by the increase of second-order rate constants (K_2) from 0.311 to 0.869 gm gmin^{-1}.

To investigate the DCF adsorption further, Langmuir and Freundlich adsorption models were used to fit the equilibrium data. As seen in Table 2 and Fig. 8, the Langmuir model fits reasonably well with the experimental data with a correlation coefficient of $R^2 > 0.98$. This means that the adsorption of DCF occurs as monolayers onto homogeneously dispersed adsorption sites on the adsorbent
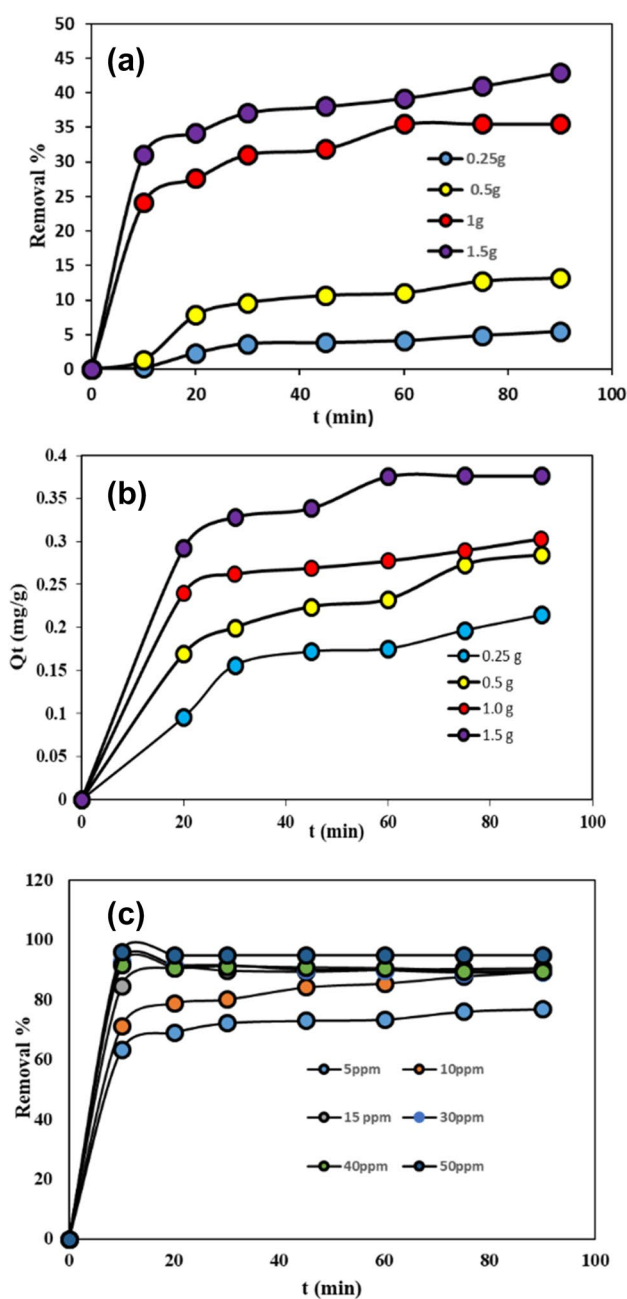

Fig. 6 **a** Effect of adsorbent mass and contact time on the removal efficiency of DCF. **b** Amount of adsorbed DCF at given contact times for different masses of the adsorbent (DCF concentration was 10 mgL^{-1}). **c** Effect of DCF concentration on the removal of DCF at pH 2 (Total liquid volume 100 mL; experiments were carried out at room temperature)

surface with absence of interaction between the adsorbed DCF molecules. The maximum amount of DCF adsorbed was 13.16 mg g^{-1} at 25 °C. Freundlich model did not fit equally well with the data based on smaller correlation coefficient (R^2: 0.95). The value of the Freundlich constant

Fig. 7 Fitting of kinetic data of DCF adsorption with (**a**) PFO kinetic model and (**b**) PSO model. (The models are fitted with different mass of the adsorbent. The initial concentration of DCF was 10 mgL^{-1}, temperature was 25 °C and total volume 100 mL.)
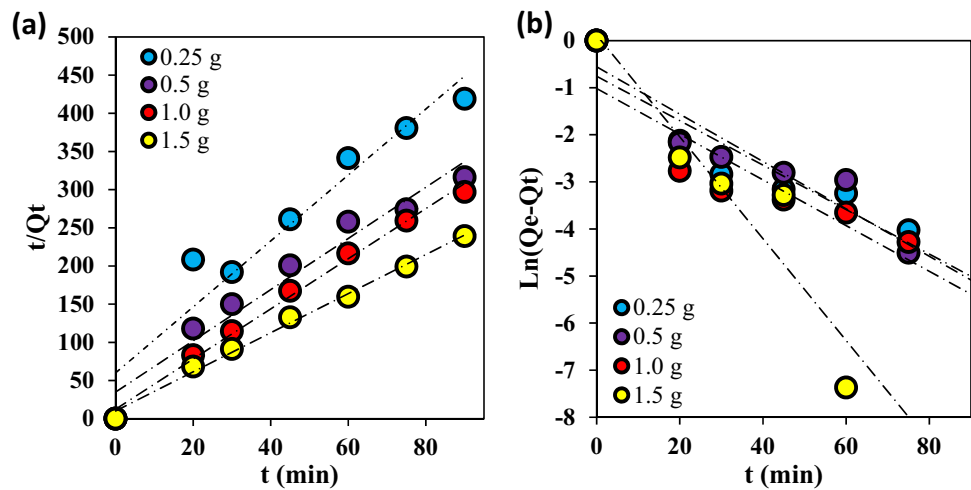

Table 1 Kinetic parameters of DCF adsorption onto hydrochar-derived adsorbent at 25 °C and 10 mgL^{-1}

Adsorbent mass (g)	$Q_{e,exp}$ (mgg^{-1})	Pseudo-first-order (PFO)			Pseudo-second-order (PSO)		
		$Q_{e,cal}$ (mgg^{-1})	K_1 (min^{-1})	R^2	$Q_{e,cal}$ (mgg^{-1})	K_2 (gmg.min^{-1})	R^2
0.25	0.214	0.470	0.108	0.850	0.231	0.311	0.930
0.5	0.284	0.951	1.278	0.883	0.298	0.322	0.958
1.0	0.303	0.953	2.340	0.785	0.304	0.646	0.993
1.5	0.376	0.898	0.274	0.880	0.391	0.869	0.993

Table 2 Langmuir and Freundlich parameters for DCF adsorption

Langmuir				Freundlich		
Q_{max} (mgg^{-1})	K_L (Lmg^{-1})	R_L	R^2	K_F (mg/g)(L/mg)$^{1/n}$	n	R^2
13.16	0.042	0.320	0.980	3.04	1.825	0.951

Fig. 8 Fitting of the experimental DCF adsorption data against (**a**) Langmuir adsorption model and (**b**) Freundlich model. (The initial concentration used in the experiment was varied between 0 and 50 mgL^{-1}, mass of adsorbent was 1.5 g, contact time 90 min, pH = 2.0 and temperature was 25 °C)
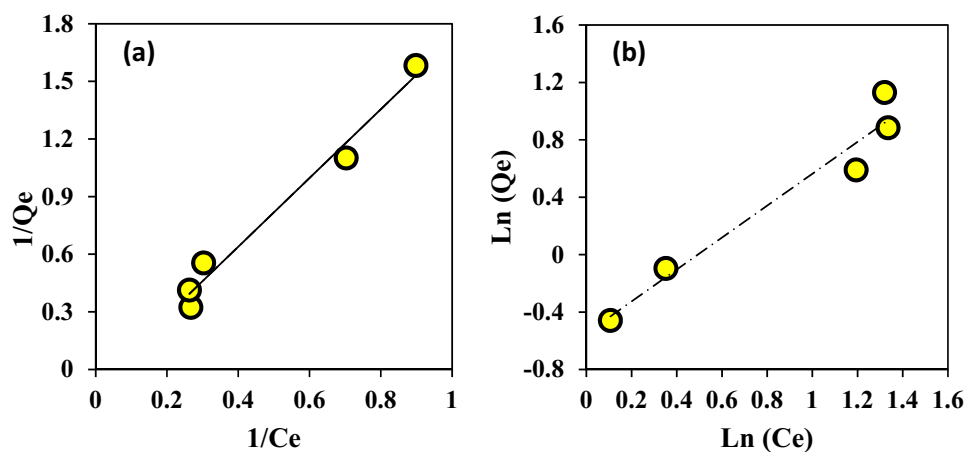
n is larger than 1 (n: 1.825), which points out the favourable adsorption conditions.

A comparison between the maximum adsorption capacity of the adsorbent prepared in this work and the values reported earlier for physically and chemically activated carbons are presented in Table 3. It can be observed that PKC (13.16 mgg^{-1}) has very good adsorption capacity in DCF adsorption compared to other adsorbents derived from lignocellulosic materials and activated especially by physical means. Higher adsorption capacities are achieved using ZnCl$_2$ and K$_2$CO$_3$ as chemical activating agents. The

Table 3 Comparison of the maximum adsorption capacity of DCF onto different adsorbents in this study and reference studies

Adsorbent	Adsorption conditions				S_{BET} (m^2g^{-1})	Q_{max} (mgg^{-1})	Refs.
	pH	C_i (mgL^{-1})	T (°C)	t (h)			
Hydrochar-derived adsorbent	2.0	0–50	25	1.5	131	13.16	This work
Orange peel activated using air	7.0	15–600	25	24	499	5.73	[48]
Olive stone activated by H_2SO_4	4.2	25–150	23	3	–	11.0	[49]
Orange peel activated by K_2CO_3	4.5	10–200	30	24	457	5.60	[50]
Orange peel activated by CO_2	7.0	15–600	25	24	301	1.91	[48]
Cyclamen persicum tubers activated by $ZnCl_2$	2.0	20–70	15	2	881	22.22	[19]
Tea waste derived carbon activated by $ZnCl_2$	6.5	10–50	30	6	865	62	[51]
Cocoa pods husks activated by H_2SO_4	7	10–30	25	0.75	not known	5	[52]
Cocoa shell activated carbon, microwave + 20% lime + 40% $FeCl_3$ + 40% $ZnCl_2$	7	10–300	25	3.7	619	63.5	[53]
Potato peel waste carbon activated by K_2CO_3	5	10–100	25	17	866	68.5	[54]

adsorption times reported for other materials have mainly been significantly longer than in our case.

The adsorption mechanism between PKC and DCF is useful to understand the performance of PKC. Despite the specific surface area of the adsorbent being only about 131 m^2g^{-1}, we obtained a good removal of 95% at pH 2. At this pH, the electrostatic interactions cannot explain the good performance of the adsorbent, since the pKa of DCF is ~ 4.2 (typical for weak acid) and at the pH of the experiment, DCF is mainly present in protonated form while the adsorbent is positively charged. The result indicates that the surface functional groups played a major role in the adsorption of DCF onto PKC. DCF molecule contains three non-polar structures—two aromatic rings and hydrocarbon chain. Diarylamine and carboxyl acid groups improve the DCF solubility in water. Diarylamine and carboxylic acid groups can form strong hydrogen bonds, while non-polar groups can create Van der Waals bonding with other non-polar groups. The aromatic rings can also create π–π interaction via aromatic stacking. The FTIR spectrum of PKC showed the presence of phenolic groups that improve the bonding between DCF and the adsorbent [55–57]. The interaction via aromatic π–π stacking and hydrogen bonding between -OH groups of phenol and carboxylic acid groups of DCF are probably the main cause for good removal at acidic pH.

Regeneration and reusability

Spent PKC was regenerated after DCF adsorption according to the protocol proposed by Zbair et al. [58, 59]. The results presented in Fig. 9 show, that PKC has a very good performance after five cycles of adsorption and regeneration. Furthermore, the removal efficiency remains steady without any significant loss in its ability to adsorb DCF. This shows that the developed adsorbent can be used several times before
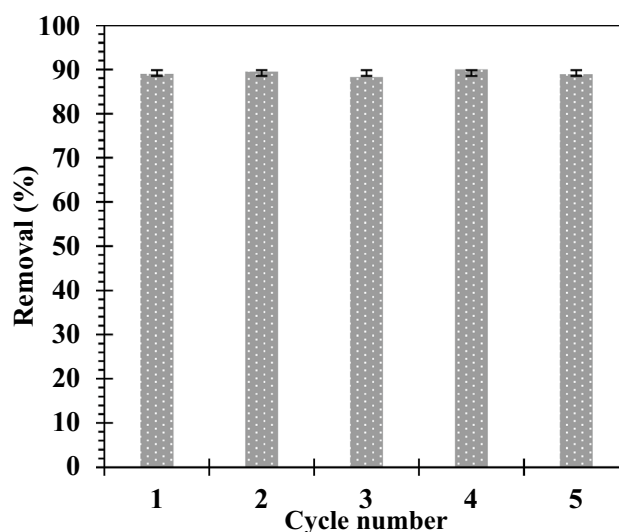

Fig. 9 Reusability of PKC adsorbent after cycles of adsorption and regeneration. (Adsorption experiments were carried out with 15 mg $^{-1}$ DCF, 1.5 g of PKC, 100 mL total volume and 25 °C temperature. Regeneration was done using 20 mL 95% ethanol.)

it loses its adsorption capacity, which is important in the practical use of the material.

Conclusions

An efficient adsorbent for diclofenac removal from water was successfully developed through hydrothermal carbonization and activation under N_2 flow. The prepared adsorbent was mesoporous and it had specific surface area of 131 m^2g^{-1}. Based on FTIR analysis, the hydrochar surface was rich in oxygen containing functional groups, while their quantity and quality decreased after activation. Activation increased the amount of graphene and graphite structures

in the material while cellulose and hemicellulose structures were removed. Maximum adsorption capacity of 13.16 mgg^{-1} for diclofenac was achieved, which is better than capacities reported in several previous works. The adsorption equilibrium followed the Langmuir model meaning that diclofenac adsorption occurs as monolayers on homogenously dispersed adsorption sites. The adsorption kinetics was explained better by pseudo-second-order kinetic model. The repeated regeneration experiments showed that the material kept high adsorption capacity even after five cycles. This study demonstrates that hydrothermal carbonization can be used as a basic process for production of an efficient hydrochar-derived adsorbent that has a good potential in the low-cost water purification applications.

Compliance with ethical standards

References

1. Wang L, Chang Y, Li A (2019) Hydrothermal carbonization for energy-efficient processing of sewage sludge: a review. Renew Sustain Energy Rev 108:423–440
2. Han L, Sun H, Ro K, Sun K, Libra J, Xing B (2017) Removal of antimony (III) and cadmium (II) from aqueous solution using animal manure-derived hydrochars and pyrochars. Biores Technol 234:77–85
3. Sharma R, Jasrotia K, Singh N, Ghosh P, Srivastava S, Sharma N, Singh J, Kanwar R, Kumar A (2019) A comprehensive review on hydrothermal carbonization of biomass and its applications. Chem Afr 3(1):1–19
4. Sun Y, Gao B, Yao Y, Fang J, Zhang M, Zhou Y, Chen H, Yang L (2014) Effects of feedstock type, production method, and pyrolysis temperature on biochar and hydrochar properties. Chem Eng J 240:574–578
5. Taskin E, de Castro Bueno C, Allegretta I, Terzano R, Rosa A, Loffredo E (2019) Multianalytical characterization of biochar and hydrochar produced from waste biomasses for environmental and agricultural applications. Chemosphere 233:422–430
6. Berge N, Li L, Flora J, Ro K (2015) Assessing the environmental impact of energy production from hydrochar generated via hydrothermal carbonization of food wastes. Waste Manage 43:203–217
7. Wang L, Guo Y, Zhu Y, Li Y, Qu Y, Rong C, Ma X, Wang Z (2010) A new route for preparation of hydrochars from rice husk. Biores Technol 101(24):9807–9810
8. Fang J, Zhan L, Ok Y, Gao B (2018) Minireview of potential applications of hydrochar derived from hydrothermal carbonization of biomass. J Ind Eng Chem 57:15–21
9. Guo N, Li M, Sun X, Wang F, Yang R (2017) Enzymatic hydrolysis lignin derived hierarchical porous carbon for supercapacitors in ionic liquids with high power and energy densities. Green Chem 19(11):2595–2602
10. Guo S, Dong X, Zhu C, Han Y, Ma F, Wu T (2017) Pyrolysis behaviors and thermodynamics properties of hydrochar from bamboo (Phyllostachys heterocycla cv. pubescens) shoot shell. Bioresour Technol 233:92–98
11. Kambo H, Dutta A (2015) A comparative review of biochar and hydrochar in terms of production, physico-chemical properties and applications. Renew Sustain Energy Rev 45:359–378
12. Puccini M, Stefanelli E, Tasca AL, Vitolo S (2018) Pollutant removal from gaseous and aqueous phases using hydrochar-based activated carbon. Chem Eng Trans 67:637–642
13. Yang D, Li Z, Liu M, Zhang X, Chen Y, Xue H, Ye E, Luque R (2019) Biomass-derived carbonaceous materials: recent progress in synthetic approaches, advantages, and applications. ACS Sustain Chem Eng 7(5):4564–4585
14. Herawan S, Hadi M, Ayob M, Putra A (2013) Characterization of activated carbons from oil-palm shell by CO$_2$ activation with no holding carbonization temperature. Sci World J 2013:1–6
15. Issabayeva G, Aroua M, Sulaiman N (2006) Removal of lead from aqueous solutions on palm shell activated carbon. Biores Technol 97(18):2350–2355
16. Lua A, Jia Q (2009) Adsorption of phenol by oil–palm-shell activated carbons in a fixed bed. Chem Eng J 150(2–3):455–461
17. Onundi Y, Mamun A, Khatib M, Ahmed Y (2010) Adsorption of copper, nickel and lead ions from synthetic semiconductor industrial wastewater by palm shell activated carbon. Int J Environ Sci Technol 7(4):751–758
18. Tan I, Ahmad A, Hameed B (2008) Adsorption of basic dye using activated carbon prepared from oil palm shell: batch and fixed bed studies. Desalination 225(1–3):13–28
19. Jodeh S, Abdelwahab F, Jaradat N, Warad I, Jodeh W (2016) Adsorption of diclofenac from aqueous solution using Cyclamen persicum tubers based activated carbon (CTAC). J Assoc Arab Univ Basic Appl Sci 20(1):32–38
20. Joss A, Keller E, Alder A, Göbel A, McArdell C, Ternes T, Siegrist H (2005) Removal of pharmaceuticals and fragrances in biological wastewater treatment. Water Res 39(14):3139–3152
21. Landry K, Boyer T (2013) Diclofenac removal in urine using strong-base anion exchange polymer resins. Water Res 47(17):6432–6444
22. Lienert J, Güdel K, Escher B (2007) Screening method for ecotoxicological hazard assessment of 42 pharmaceuticals considering human metabolism and excretory routes. Environ Sci Technol 41(12):4471–4478
23. Thanhmingliana T, Tiwari D (2015) Efficient use of hybrid materials in the remediation of aquatic environment contaminated with micro-pollutant diclofenac sodium. Chem Eng J 263:364–373
24. Mehinto A, Hill E, Tyler C (2010) Uptake and biological effects of environmentally relevant concentrations of the nonsteroidal anti-inflammatory pharmaceutical diclofenac in rainbow trout (Oncorhynchus mykiss). Environ Sci Technol 44(6):2176–2182

25. Vergili I (2013) Application of nanofiltration for the removal of carbamazepine, diclofenac and ibuprofen from drinking water sources. J Environ Manag 127:177–187

26. Antero R, Alves A, Ferreira Sales P, de Oliveira S, Ojala S, Brum S (2019) A new approach to obtain mesoporous-activated carbon via hydrothermal carbonization of Brazilian Cerrado biomass combined with physical activation for bisphenol-a removal. Chem Eng Commun 206(11):1498–1514

27. Langmuir I (1916) The constitution and fundamental properties of solids and liquids. Part I Solids. J Am Chem Soc 252:2221–95. https://doi.org/10.1021/ja02268a002

28. Freundlich H (1906) Über die adsorption in lösungen. Zeitschrift Für Phys Chemie 57A:385

29. Lagergren S, B. S (1898) Zur theorie der sogenannten adsorption geloester stoffe. Veternskapsakad Handl. 24:1–39

30. Liu Y (2008) New insights into pseudo-second-order kinetic equation for adsorption. Coll Surf A Physicochem Eng Asp 320:275–8

31. Smith A, Singh S, Ross A (2016) Fate of inorganic material during hydrothermal carbonisation of biomass: influence of feedstock on combustion behaviour of hydrochar. Fuel 169:135–145

32. Hamza U, Nasri N, Amin N, Mohammed J, Zain H (2015) Characteristics of oil palm shell biochar and activated carbon prepared at different carbonization times. Desalination Water Treat 57(17):7999–8006

33. Bazan A, Nowicki P, Półrolniczak P, Pietrzak R (2016) Thermal analysis of activated carbon obtained from residue after supercritical extraction of hops. J Therm Anal Calorim 125(3):1199–1204

34. Zbair M, Bottlinger M, Ainassaari K, Ojala S, Stein O, Keiski RL et al (2018) Hydrothermal carbonization of argan nut shell: functional mesoporous carbon with excellent performance in the adsorption of bisphenol A and diuron. Waste Biomass Valoriz. https://doi.org/10.1007/s12649-018-00554-0

35. Ulfah M, Raharjo S, Hastuti P, Darmadji P (2016) The potential of palm kernel shell activated carbon as an adsorbent for β-carotene recovery from crude palm oil. AIP Conf Proc 1755:130016

36. Siipola V, Tamminen T, Källi A, Kupila R, Romar H, Rasa K, Keskinen R, Hyväluoma J, Hannula M, Wikberg H (2018) Effects of biomass type, carbonization process, and activation method on the properties of bio-based activated carbons. BioResources 13:3

37. Hidayu A, Sukor M, Mohammad N, Elham O, Azri N, Azhar M, Jalil M (2019) Preparation of activated carbon from palm kernel shell by chemical activation and its application for β-carotene adsorption in crude palm oil. J Phys Conf Ser 1349:012103

38. Pal T, Paul S, Sa B (2011) Polymethylmethacrylate coated alginate matrix microcapsules for controlled release of diclofenac sodium. Pharmacol Pharm 02(02):56–66

39. Nicholas A, Hussein M, Zainal Z, Khadiran T (2018) Palm kernel shell activated carbon as an inorganic framework for shape-stabilized phase change material. Nanomaterials 8(9):689

40. Majdoub M, Essamlali Y, Amadine O, Ganetri I, Zahouily M (2019) Organophilic graphene nanosheets as a promising nanofiller for bio-based polyurethane nanocomposites: investigation of the thermal, barrier and mechanical properties. New J Chem 43(39):15659–15672

41. Nanda S, Mohanty P, Pant K, Naik S, Kozinski J, Dalai A (2012) Characterization of North American lignocellulosic biomass and biochars in terms of their candidacy for alternate renewable fuels. BioEnergy Res 6(2):663–677

42. Pardanaud C, Cartry G, Lajaunie L, Arenal R, Buijnsters J (2019) Investigating the possible origin of Raman bands in defective sp2/sp3 carbons below 900 cm−1: phonon density of states or double resonance mechanism at play? C J Carbon Res 5(4):79

43. RRUFF (2020). An integrated database for Raman, X-ray diffraction and chemistry data for minerals. Available online at: www.ffuff.info (retrieved on 24.11.2020)

44. Ramesh T, Rajalakshmi N, Kaveripatnam S, Dhathathreyan (2017) Synthesis and characterization of activated carbon from jute fibers for hydrogen storage. Renew Energy Environ Sustain 2:4. https://doi.org/10.1051/rees/2017001

45. Johra FT, Lee J-W, Jung W-G (2014) Facile and safe graphene preparation on solution based platform. J Ind Eng Chem 20:2883–2887. https://doi.org/10.1016/j.jiec.2013.11.022

46. Zhang K, Zhang Y, Wang S (2014) Enhancing thermoelectric properties of organic composites through hierarchical nanostructures. Sci Rep. https://doi.org/10.1038/srep03448

47. Yang Y, Chun Y, Sheng G, Huang M (2004) pH-Dependence of pesticide adsorption by wheat-residue-derived black carbon. Langmuir 20(16):6736–6741

48. Fernandez ME, Ledesma B, Román S, Bonelli PR, Cukierman AL (2015) Development and characterization of activated hydrochars from orange peels as potential adsorbents for emerging organic contaminants. Bioresour Technol 183:221–228. https://doi.org/10.1016/j.biortech.2015.02.035

49. Larous S, Meniai AH (2016) Adsorption of Diclofenac from aqueous solution using activated carbon prepared from olive stones. Int J Hydrogen Energy 41:10380–10390. https://doi.org/10.1016/j.ijhydene.2016.01.096

50. Tomul F, Arslan Y, Başoğlu FT, Babuçcuoğlu Y, Tran HN (2019) Efficient removal of anti-inflammatory from solution by Fe-containing activated carbon: adsorption kinetics, isotherms, and thermodynamics. J Environ Manag 238:296–306. https://doi.org/10.1016/j.jenvman.2019.02.088

51. Malhotra M, Suresh S, Garg A (2018) Tea waste derived activated carbon for the adsorption of sodium diclofenac from wastewater: adsorbent characteristics, adsorption isotherms, kinetics, and thermodynamics. Environ Sci Pollut Res 25(32):32210–32220

52. de Luna M, Murniati BW, Rivera K, Arazo R (2017) Removal of sodium diclofenac from aqueous solution by adsorbents derived from cocoa pod husks. J Environ Chem Eng 5(2):1465–1474

53. Saucier C, Adebayo M, Lima E, Cataluña R, Thue P, Prola L, Puchana-Rosero M, Machado F, Pavan F, Dotto G (2015) Microwave-assisted activated carbon from cocoa shell as adsorbent for removal of sodium diclofenac and nimesulide from aqueous effluents. J Hazard Mater 289:18–27

54. Bernardo M, Rodrigues S, Lapa N, Matos I, Lemos F, Batista M, Carvalho A, Fonseca I (2016) High efficacy on diclofenac removal by activated carbon produced from potato peel waste. Int J Environ Sci Technol 13(8):1989–2000

55. Mao N, Huang L, Shuai Q (2019) Facile synthesis of porous carbon for the removal of diclofenac sodium from water. ACS Omega 4(12):15051–15060

56. Schames J, Henchman R, Siegel J, Sotriffer C, Ni H, McCammon J (2004) Discovery of a novel binding trench in HIV integrase. J Med Chem 47(8):1879–1881

57. Chen W, Duan L, Zhu D (2007) Adsorption of polar and nonpolar organic chemicals to carbon nanotubes. Environ Sci Technol 41(24):8295–8300

58. Zbair M, Ainassaari K, El Assal Z, Ojala S, El Ouahedy N, Keiski RL et al (2018) Steam activation of waste biomass: highly microporous carbon, optimization of bisphenol A, and diuron adsorption by response surface methodology. Environ Sci Pollut Res 25:35657–35671. https://doi.org/10.1007/s11356-018-3455-3

59. Zbair M, Ainassaari K, Drif A, Ojala S, Bottlinger M, Pirilä M et al (2018) Toward new benchmark adsorbents: preparation and characterization of activated carbon from argan nut shell for bisphenol a removal. Environ Sci Pollut Res. https://doi.org/10.1007/s11356-017-0634-6

Authors and Affiliations

Velma Beri Kimbi Yaah[1] · Mohamed Zbair[2] · Sérgio Botelho de Oliveira[3] · Satu Ojala[1] [ORCID]

✉ Satu Ojala
satu.ojala@oulu.fi

[1] Environmental and Chemical Engineering Research Unit, Faculty of Technology, University of Oulu, Oulu, Finland

[2] Laboratory of Catalysis and Corrosion of Materials (LCCM), Faculty of Sciences, University of Chouaib Doukkali, El Jadida, Morocco

[3] Federal Institute of Goiás - IFG, Goiania, Brazil